

Dynamical generation of the scalar $f_0(500)$, $f_0(980)$, and $K_0^*(700)$ resonances in the $D_s^+ \rightarrow K^+ \pi^+ \pi^-$ reaction

L. R. Dai^{1,2,*} and E. Oset^{2,†}¹*School of Science, Huzhou University, Huzhou 313000, Zhejiang, China*²*Departamento de Física Teórica and IFIC, Centro Mixto Universidad de Valencia-CSIC Institutos de Investigación de Paterna, Apartado 22085, 46071 Valencia, Spain* (Received 10 August 2023; accepted 16 February 2024; published 5 March 2024)

We develop a model aimed at understanding the three mass distributions of pairs of mesons in the Cabibbo-suppressed $D_s^+ \rightarrow K^+ \pi^+ \pi^-$ decay recently measured with high statistics by the BESIII collaboration. The largest contributions to the process come from the $D_s^+ \rightarrow K^+ \rho^0$ and $D_s^+ \rightarrow K^{*0} \pi^+$ decay modes, but the $D_s^+ \rightarrow K_0^*(1430) \pi^+$ and $D_s^+ \rightarrow K^+ f_0(1370)$ modes also play a moderate role and all of them are introduced empirically. Instead, the contribution of the $f_0(500)$, $f_0(980)$, and $K_0^*(700)$ resonances is introduced dynamically by looking at the decay modes at the quark level, hadronizing $q\bar{q}$ pairs to give two mesons, and allowing these mesons to interact, for which we follow the chiral unitary approach, to finally produce the $K^+ \pi^+ \pi^-$ final state. While the general features of the mass distributions are fairly obtained, we pay special attention to the specific effects created by the light scalar resonances, which are visible in the low mass region of the $\pi^+ \pi^-$ ($f_0(500)$) and $K^+ \pi^-$ ($K_0^*(700)$) mass distributions and a narrow peak for $\pi^+ \pi^-$ distribution corresponding to $f_0(980)$ excitation. The contribution of these three resonances is generated by only one parameter. We see the agreement found in these regions as further support for the nature of the light scalar states as dynamically generated from the interaction of pseudoscalar mesons.

DOI: [10.1103/PhysRevD.109.054008](https://doi.org/10.1103/PhysRevD.109.054008)

I. INTRODUCTION

The hadronic weak decays of D, D_s mesons are an excellent source of information on the interaction of hadrons [1–14]. In particular, decays of D, D_s into three mesons allow one to study the interaction of pairs of particles at different invariant masses and observe hadronic resonances. One case which has attracted much attention is the decay with one kaon in the final state, in particular the golden channel, $D \rightarrow K\pi\pi$ has been thoroughly studied [15–28]. The related $D^0 \rightarrow K^- \pi^+ \eta$ reaction has been studied in Ref. [29]. Similar work to the one done here on $D_s \rightarrow KK\pi$ is also addressed in [30–34] and $D \rightarrow KKK$ is also addressed in [35–37]. In the present work we study the singly Cabibbo-suppressed $D_s \rightarrow K^+ \pi^+ \pi^-$ decay.

The reaction has been measured in [38] by the FOCUS collaboration and more recently, with better statistics, by the BESIII collaboration in [39]. In this reaction, in

addition to the dominant mode $D_s^+ \rightarrow K^+ \rho, \rho \rightarrow \pi^+ \pi^-$ and $D_s^+ \rightarrow K^*(892)^0 \pi^+, K^*(892)^0 \rightarrow K^+ \pi^-$, the experiment finds traces of the $f_0(500)$, $f_0(980)$, and $f_0(1370)$ resonances. No theoretical work on this particular channel is available to the best of our knowledge, and we wish to address this problem here.

Our aim is to use the theoretical tools provided by the chiral unitary approach [40] to relate the production of the $f_0(500)$, $f_0(980)$, and $K_0^*(700)$ scalar resonances. In this framework the $f_0(500)$, $f_0(980)$ resonances appear from the interaction of the $\pi\pi$, $K\bar{K}$, $\eta\eta$ channels and the $K_0^*(700)$ resonance is produced by the interaction of the $K\eta$ and $K\pi$ channels. Hence, our reaction mechanism consists in first producing these channels from the weak decay and later implement the final state interaction of these channels from where the resonances emerge. The procedure to produce these mesons follows closely the work done in Refs. [24,30–34]. One looks at the main production modes at the quark level based on external and internal emission [41], and then proceeds with the hadronization of the $q\bar{q}$ pairs in order to produce the coupled channels needed to generate these resonances. One keeps the terms where these channels are produced and implements the final state interaction such that the observed channels in the experiment are generated. The nice thing is that we can correlate the production of these resonances by means of only one

*dailianrong@zjhu.edu.cn

†oset@ific.uv.es

Published by the American Physical Society under the terms of the [Creative Commons Attribution 4.0 International license](https://creativecommons.org/licenses/by/4.0/). Further distribution of this work must maintain attribution to the author(s) and the published article's title, journal citation, and DOI. Funded by SCOAP³.

parameter, measuring the relative strength of the internal to external emission, which comes from a fit to the data but should respect the $1/N_c$ reduction in the amplitude of internal to external emission. This procedure is different from the one normally adopted in experimental analyses where the production of each of these resonances is parametrized and fitted to the data. Hence, our approach is very restrictive, and the eventual agreement with the data comes to support the picture of these resonances as being dynamically generated from the interaction of pseudoscalar mesons, which is the aim of the present work. We find indeed a fair agreement with the data in the region where these resonances appear, the low energy region in the $\pi\pi$ mass distribution for the $f_0(500)$, a narrow peak for the $f_0(980)$ in the $\pi\pi$ distribution, and the low energy region in the $K\pi$ distribution for the $K_0^*(700)$.

II. FORMALISM

The formalism includes different steps that we will summarize below. In the first one we look at the different topologies that can contribute to this Cabibbo-suppressed process at the quark level. In Figs. 1 and 3 we look into external and internal emission producing a pseudoscalar and a vector. In Fig. 1 we produce a π^+ and K^{*0} with external emission, and the latter can decay into $K^+\pi^-$ which is one of the important modes observed in the BESIII experiment [39]. In Fig. 3, by means of internal emission we produce a ρ^0 meson and a K^+ , and the ρ^0 can decay to $\pi^+\pi^-$, again one important mode observed in the BESIII experiment [39].

Next we look at the production of three pseudoscalar mesons. This is accomplished by hadronizing a $q\bar{q}$ component into two pseudoscalar mesons. In Fig. 2 a K^+ is produced in external emission and the $s\bar{s}$ component is hadronized into two pseudoscalars. In Fig. 5, again with external emission, a π^+ is produced and the $d\bar{s}$ component is hadronized into two pseudoscalars. In Fig. 4 the mechanism proceeds via internal emission, a K^+ is produced and the $s\bar{s}$ component is hadronized into two pseudoscalars. In Fig. 6, again with internal emission a K^+ is produced and the $d\bar{d}$ component is hadronized into two pseudoscalars.

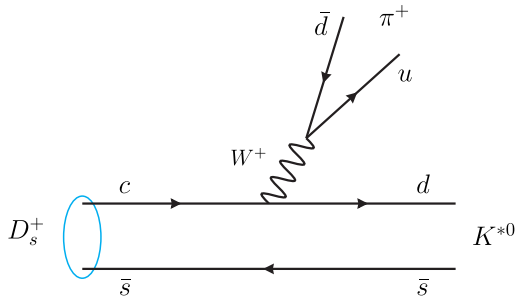


FIG. 1. Mechanism for production of π^+K^{*0} in D_s^+ decay with external emission.

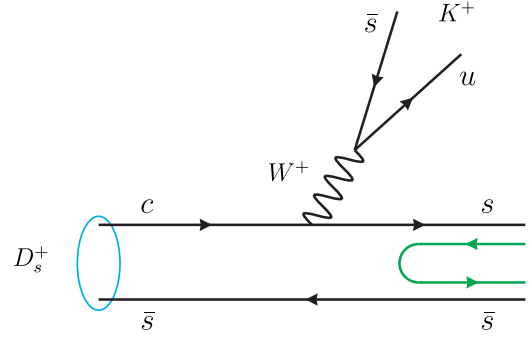


FIG. 2. $D_s^+ \rightarrow K^+s\bar{s}$ with external emission and $s\bar{s}$ hadronization.

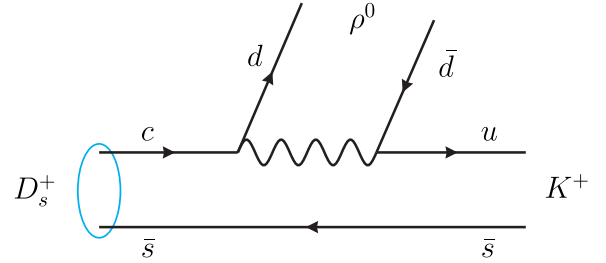


FIG. 3. Mechanism for $D_s^+ \rightarrow \rho K^+$ with internal emission.

The fact that we have a Cabibbo-suppressed decay increases the number of diagrams with respect to a Cabibbo-favored process like in [24]. Indeed, in Fig. 2 the Cabibbo-suppressed vertex appears in the upper part of the W^+ exchange, $W\bar{s}u$ vertex, while in Fig. 5 the Cabibbo-suppressed vertex appears in the lower part of the W exchange, $Wc\bar{d}$ vertex. Both vertices imply the same reduction factor, $\sin\theta_c$. We have a similar situation with diagrams 4 and 6. We consider all these mechanisms and we give a weight to the different diagrams according to the following scheme:

- (1) weight α for K^{*0} production,
- (2) weight ah , the h factor accounting for the mechanism of hadronization,
- (3) weight γ for ρ^0 production,
- (4) weight γh since it involves an extra hadronization as in the case of (2),

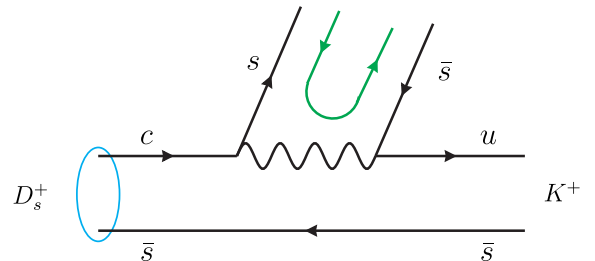
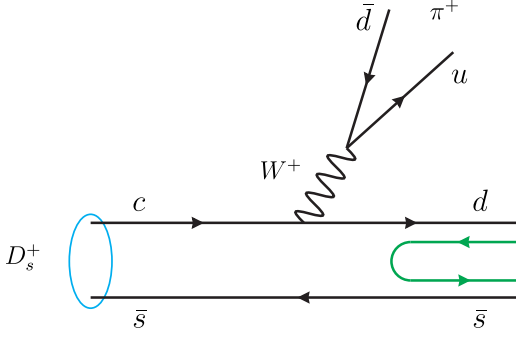


FIG. 4. $D_s^+ \rightarrow K^+s\bar{s}$ with internal emission followed by $s\bar{s}$ hadronization.

FIG. 5. $D_s^+ \rightarrow \pi^+ d \bar{s}$ with external emission and $d \bar{s}$ hadronization.

- (5) weight ah since it has the same topology as the case of (2), and
- (6) weight γh since it involves an extra hadronization with respect to case of (3).

Next we proceed to look in detail into the different hadronization processes. In Figs. 2 and 4 we have the hadronization of the $s\bar{s}$ component and we add a $\bar{q}q$ pair with the quantum numbers of the vacuum. By writing the $q_i \bar{q}_j$ matrix of SU(3) in terms of the pseudoscalar mesons we have

$$q\bar{q} \rightarrow P = \begin{pmatrix} \frac{\pi^0}{\sqrt{2}} + \frac{\eta}{\sqrt{3}} & \pi^+ & K^+ \\ \pi^- & -\frac{\pi^0}{\sqrt{2}} + \frac{\eta}{\sqrt{3}} & K^0 \\ K^- & \bar{K}^0 & -\frac{\eta}{\sqrt{3}} \end{pmatrix}, \quad (1)$$

where we have taken the standard η and η' mixing of Ref. [42] and neglected the η' which does not play a role in the generation of the resonances that we shall discuss. Then

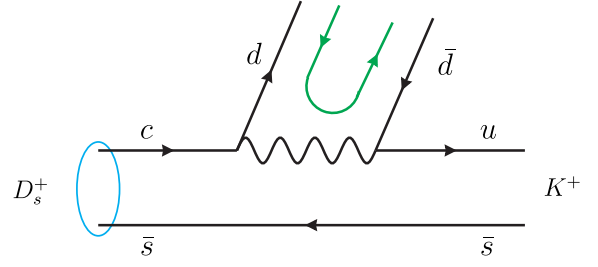
$$\begin{aligned} s\bar{s} &\rightarrow \sum_i s\bar{q}_i q_i \bar{s} = \sum_i P_{3i} P_{i3} = (P^2)_{33} \\ &= K^- K^+ + \bar{K}^0 K^0 + \frac{1}{3} \eta\eta \end{aligned} \quad (2)$$

In Fig. 5 we have the hadronization of $d\bar{s}$ as

$$\begin{aligned} d\bar{s} &\rightarrow \sum_i d\bar{q}_i q_i \bar{s} = \sum_i P_{2i} P_{i3} = (P^2)_{23} \\ &= \pi^- K^+ - \frac{1}{\sqrt{2}} \pi^0 K^0. \end{aligned} \quad (3)$$

In Fig. 6 we have the hadronization of $d\bar{d}$ as

$$\begin{aligned} d\bar{d} &\rightarrow \sum_i d\bar{q}_i q_i \bar{d} = (P^2)_{22} \\ &= \pi^- \pi^+ + \frac{\pi^0 \pi^0}{\sqrt{2}} + \frac{\eta\eta}{3} - \frac{2}{\sqrt{6}} \pi^0 \eta \\ &\quad + K^0 \bar{K}^0 \end{aligned} \quad (4)$$

FIG. 6. $D_s^+ \rightarrow K^+ d \bar{d}$ with internal emission and $d \bar{d}$ hadronization.

The (4) and (6) cases correspond to the same topology and have the same weight and can be summed into

$$\begin{aligned} (4) + (6) &\rightarrow (P^2)_{33} + (P^2)_{22} \\ &= \pi^+ \pi^- + \frac{\pi^0 \pi^0}{\sqrt{2}} + \frac{2}{3} \eta\eta + K^+ K^- + 2K^0 \bar{K}^0 \\ &\quad - \sqrt{\frac{2}{3}} \pi^0 \eta. \end{aligned} \quad (5)$$

We can see that in Fig. 6 we already obtain $K^+ \pi^- \pi^+$ at the tree level, but we also get other intermediate states that upon rescattering lead to the same state, as depicted in Fig. 7.

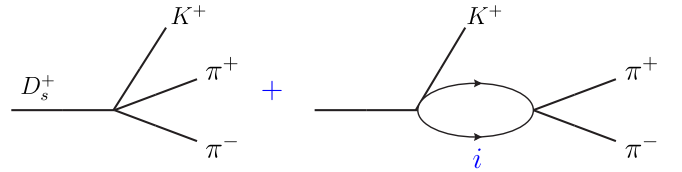
Given Eqs. (2)–(5), we can write the production matrix for each mechanism of Figs. 1–6.

$$t^{(2)} = \sum_i \alpha h W_i G_i(M_{\text{inv}}, \pi\pi) t_{i, \pi^+ \pi^-}(M_{\text{inv}}, \pi\pi), \quad (6)$$

where G_i are the meson-meson loop functions and $t_{i, \pi^+ \pi^-}$ the scattering matrices for transitions of the state i in the loop to the $\pi^+ \pi^-$ final state. The possible i intermediate states are $i = K^+ K^-, K^0 \bar{K}^0, \eta\eta$, and the weights W_i are given by means of Eq. (2) as

$$W_{K^+ K^-} = 1, \quad W_{K^0 \bar{K}^0} = 1, \quad W_{\eta\eta} = \frac{2}{3} \frac{1}{\sqrt{2}}.$$

In the case of the two identical particles $\eta\eta$ we have considered the factor 2 for the two particles and $\frac{1}{\sqrt{2}}$ because we work with the unitary normalization where the state is normalized as $\frac{1}{\sqrt{2}} \eta\eta$ to avoid double counting in the G loop

FIG. 7. Direct $K^+ \pi^- \pi^+$ production (tree level) and production through intermediate states, $i = \pi^+ \pi^-, \pi^0 \pi^0, \eta\eta, \pi^0 \eta, K^+ K^-, K^0 \bar{K}^0$ in general.

function. The $t_{i,j}$ transition scattering matrices are calculated with the six pseudoscalar pairs, $\pi^+\pi^-$, $\pi^0\pi^0$, K^+K^- , $K^0\bar{K}^0$, $\eta\eta$, $\pi^0\eta$ obtained in a coupled channel formalism as

$$t = [1 - VG]^{-1}V \quad (7)$$

with the transition potentials V_{ij} obtained from [43]. For the π^-K^+ and π^0K^0 interaction we use Eq. (7) with the coupled channels π^-K^+ , π^0K^0 , ηK^0 with the transition potentials of Ref. [24,29].

The G function in Eq. (7) is the diagonal matrix $\text{diag}(G_i)$ with G_i calculated with cutoff regularization as

$$G(s) = \int_{|q| < q_{\max}} \frac{d^3q}{(2\pi)^3} \frac{\omega_1 + \omega_2}{2\omega_1\omega_2} \frac{1}{s - (\omega_1 + \omega_2)^2 + i\epsilon}, \quad (8)$$

where $\omega_j = \sqrt{q^2 + m_j^2}$ ($j = 1, 2$) calculated for each channel i . We use $q_{\max} = 600$ MeV as in [43].

Similarly, we obtain

$$t^{(4+6)} = \gamma h \left\{ 1 + \sum_i W'_i G_i(M_{\text{inv}}, \pi\pi) t_{i,\pi^+\pi^-}(M_{\text{inv}}, \pi\pi) \right\} \quad (9)$$

with $i = \pi^+\pi^-, \pi^0\pi^0, K^+K^-, K^0\bar{K}^0, \eta\eta, \pi^0\eta$ and

$$\begin{aligned} W'_{\pi^+\pi^-} &= 1, & W'_{\pi^0\pi^0} &= 2 \frac{1}{2\sqrt{2}}, & W'_{K^+K^-} &= 1 \\ W'_{K^0\bar{K}^0} &= 2, & W'_{\eta\eta} &= \frac{2}{3} \frac{1}{\sqrt{2}} 2, & W'_{\pi^0\eta} &= -\sqrt{\frac{2}{3}} \end{aligned} \quad (10)$$

$$t^{(5)} = \alpha h \left\{ 1 + \sum_i \tilde{W}_i G_i(M_{\text{inv}}, \pi^-K^+) t_{i,\pi^-K^+}(M_{\text{inv}}, \pi^-K^+) \right\} \quad (11)$$

with $i = \pi^-K^+, \pi^0K^0$ and

$$\tilde{W}_{\pi^-K^+} = 1, \quad \tilde{W}_{\pi^0K^0} = -\frac{1}{\sqrt{2}}. \quad (12)$$

Note that in Eqs. (9) and (11) we have the term 1 in the amplitude, which corresponds to the tree level $K^+\pi^+\pi^-$ production. This term is absent in Eq. (6) since the primary production does not contain $K^+\pi^+\pi^-$.

It should be noted that we only consider the interaction of pairs and disregard terms of three body interaction. This is a common procedure in this kind of calculations [24,30–34]. The rationale behind it is that once a resonance has been produced in the first interaction of a pair, the phase space drastically reduces the chances that another resonance is formed in the rescattering of another pair. For instance, take the second diagram of Fig. 7 where the $f_0(500)$ is formed when producing the $\pi^+\pi^-$. It is easy to

see that the $K^+\pi^-$ invariant mass peaks around 1360 MeV, which is very far away from the peak of the $K_0^*(700)$ resonance.

A. Vector resonance production

We look now to the mechanisms of Figs. 1 and 3 for K^{*0} and ρ^0 production respectively. We show these processes in Figs. 8 and 9 respectively, including the K^{*0} and ρ^0 decays. By means of the decay of the vectors we have $K^+\pi^+\pi^-$ in the final state in both cases.

In order to obtain the $K^{*0} \rightarrow K^+\pi^-$ and $\rho^0 \rightarrow \pi^+\pi^-$ vertices we use the standard Lagrangian [44–47].

$$\mathcal{L} = -ig \langle [P, \partial_\mu P] V^\mu \rangle,$$

$$g = \frac{M_V}{2f} (M_V = 800 \text{ MeV}, f = 93 \text{ MeV}) \quad (13)$$

with $\langle \rangle$ indicating the SU(3) trace, P from Eq. (1) and V^μ given by

$$V^\mu = \begin{pmatrix} \frac{\rho^0}{\sqrt{2}} + \frac{\omega}{\sqrt{2}} & \rho^+ & K^{*+} \\ \rho^- & -\frac{\rho^0}{\sqrt{2}} + \frac{\omega}{\sqrt{2}} & K^{*0} \\ K^{*-} & \bar{K}^{*0} & \phi \end{pmatrix}. \quad (14)$$

The vertices $D_s^+ \rightarrow K^+\rho^0$ and $D_s^+ \rightarrow \pi^+K^{*0}$ have the same structure and we take

$$\begin{aligned} V_{D_s^+ \rightarrow K^+\rho^0} &\equiv \epsilon^\nu (P_{D_s^+} + P_{K^+})_\nu, \\ V_{D_s^+ \rightarrow \pi^+K^{*0}} &\equiv \epsilon^\nu (P_{D_s^+} + P_{\pi^+})_\nu \end{aligned} \quad (15)$$

up to a normalization which is included in the coefficients α, γ . Following the lines detailed in Ref. [29] we can write the amplitude in terms of the invariant masses s_{12}, s_{13}, s_{23} for the particles in the order $\pi^-(1), \pi^+(2), K^+(3)$ as (see Sec. 2.1 of Ref. [29] for the derivation)

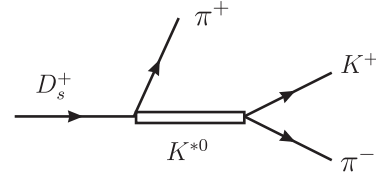


FIG. 8. Mechanism for $D_s^+ \rightarrow \pi^+K^{*0}, K^{*0} \rightarrow K^+\pi^-$.

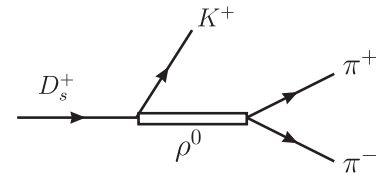


FIG. 9. Mechanism for $D_s^+ \rightarrow K^+\rho^0, \rho^0 \rightarrow \pi^+\pi^-$.

$$t^{(1)} = \alpha g \frac{1}{s_{13} - m_{K^*}^2 + im_{K^*}\Gamma_{K^*}} \times \left\{ -s_{23} + s_{12} + \frac{(m_{K^+}^2 - m_{\pi^-}^2)(m_{D_s}^2 - m_{\pi^+}^2)}{m_{K^*}^2} \right\}, \quad (16)$$

where $s_{13} = (P_{\pi^-} + P_{K^+})^2$, $s_{12} = (P_{\pi^-} + P_{\pi^+})^2$, $s_{23} = (P_{\pi^+} + P_{K^+})^2$, and similarly

$$t^{(3)} = \gamma g \sqrt{2} \frac{1}{s_{12} - m_{\rho}^2 + im_{\rho}\Gamma_{\rho}} \{-s_{13} + s_{23}\} \quad (17)$$

and we use the relationship

$$s_{12} + s_{23} + s_{13} = m_{D_s}^2 + m_{K^+}^2 + m_{\pi^+}^2 + m_{\pi^-}^2. \quad (18)$$

The masses and widths of the ρ and K^* are taken from the PDG [48].

B. Higher mass scalar resonances

Following the analysis of the experimental work [39], we also allow the contribution of two scalar resonances, the $f_0(1370)$ and $K_0^*(1430)$. These resonances do not come from pseudoscalar-pseudoscalar interaction but, instead, they are obtained from vector-vector interaction in the chiral unitary approach, together with many other states with $J = 0, 1, 2$ [49,50]. Even if the main building blocks are a pair of vector mesons, they also couple to two pseudoscalars. This is taken into account in [49,50] by means of box diagrams (see Fig. 10 of [49] and Fig. 2 of [50]), and it is seen that these diagrams have a negligible influence in the mass of the states, but they contribute to the decay of the generated states into two pseudoscalars. Yet, these are the two resonances which are obtained with less precision in [49,50], with 150–200 MeV difference in the mass with respect to the experiment. Hence, here we do not try to obtain them in the way we have dealt with the light scalar resonances and introduce them empirically with weights as free parameters.

The mechanisms for the production of these resonances are depicted in Figs. 10 and 11, and their amplitudes can be parameterized by means of

$$t^{(7)} = \beta \frac{m_{D_s}^2}{s_{13} - m_{K_0^*(1430)}^2 + im_{K_0^*(1430)}\Gamma_{K_0^*(1430)}} \quad (19)$$

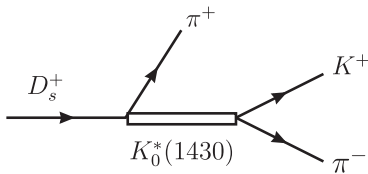


FIG. 10. Mechanism for $D_s^+ \rightarrow \pi^+ K_0^*(1430)$, $K_0^*(1430) \rightarrow K^+ \pi^-$.

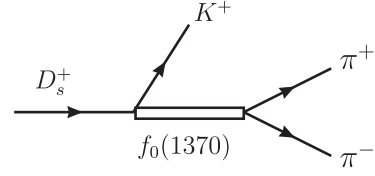


FIG. 11. Mechanism for $D_s^+ \rightarrow K^+ f_0(1370)$, $f_0(1370) \rightarrow \pi^+ \pi^-$.

for $K_0^*(1430)$ production and

$$t^{(8)} = \delta \frac{m_{D_s}^2}{s_{12} - m_{f_0(1370)}^2 + im_{f_0(1370)}\Gamma_{f_0(1370)}} \quad (20)$$

for $f_0(1370)$ production, where the factor $m_{D_s}^2$ is introduced to have β, δ dimensionless. We take the masses and widths from the PDG [48], $M = 1425$ MeV, $\Gamma = 270$ MeV for $K_0^*(1430)$ meson, and $M = 1370$ MeV, $\Gamma = 350$ MeV for $f_0(1370)$ meson.

The sum of all contributions is given by

$$t = t^{(1)} + t^{(3)} + t^{(2)} + t^{(4+6)} + t^{(5)} + t^{(7)} + t^{(8)} \quad (21)$$

and to get the mass distribution we use the PDG formula [48]

$$\frac{d^2\Gamma}{dm_{12}^2 dm_{23}^2} = \frac{1}{(2\pi)^3} \frac{1}{32M_{D_s}^3} |t|^2, \quad (22)$$

where $m_{12}^2 = s_{12}$, $m_{23}^2 = s_{23}$ for $\pi^+ \pi^-$, $\pi^+ K^+$ respectively. We integrate Eq. (22) over s_{23} with the limits of the PDG [48] and obtain $d\Gamma/dm_{12}^2$. By cyclical permutation of the indices we easily obtain $d\Gamma/dm_{13}^2$ and $d\Gamma/dm_{23}^2$.

III. RESULTS

We conduct a best fit with MINUIT to the three invariant mass distributions of Ref. [39] and we get the values for the parameters

$$\begin{aligned} \alpha &= 14.67 \pm 1.28, & h &= 6.86 \pm 2.57, \\ \gamma &= 10.75 \pm 2.31, & \beta &= -33.23 \pm 24.85, \\ \delta &= -58.84 \pm 31.27 \end{aligned} \quad (23)$$

The errors in the parameters from the MINUIT output are not small in some cases, but this is not surprising since when having many parameters there are also correlations between these parameters, and this is what the MINUIT errors reflect. The important output are the values of the observables, in this case the mass distributions.

The results for the mass distributions are shown in Fig. 12. The agreement with the data is relatively fair and the K^{*0}, ρ^0 peaks are prominent in the reaction. The $\chi^2/\text{d.o.f.}$ that we

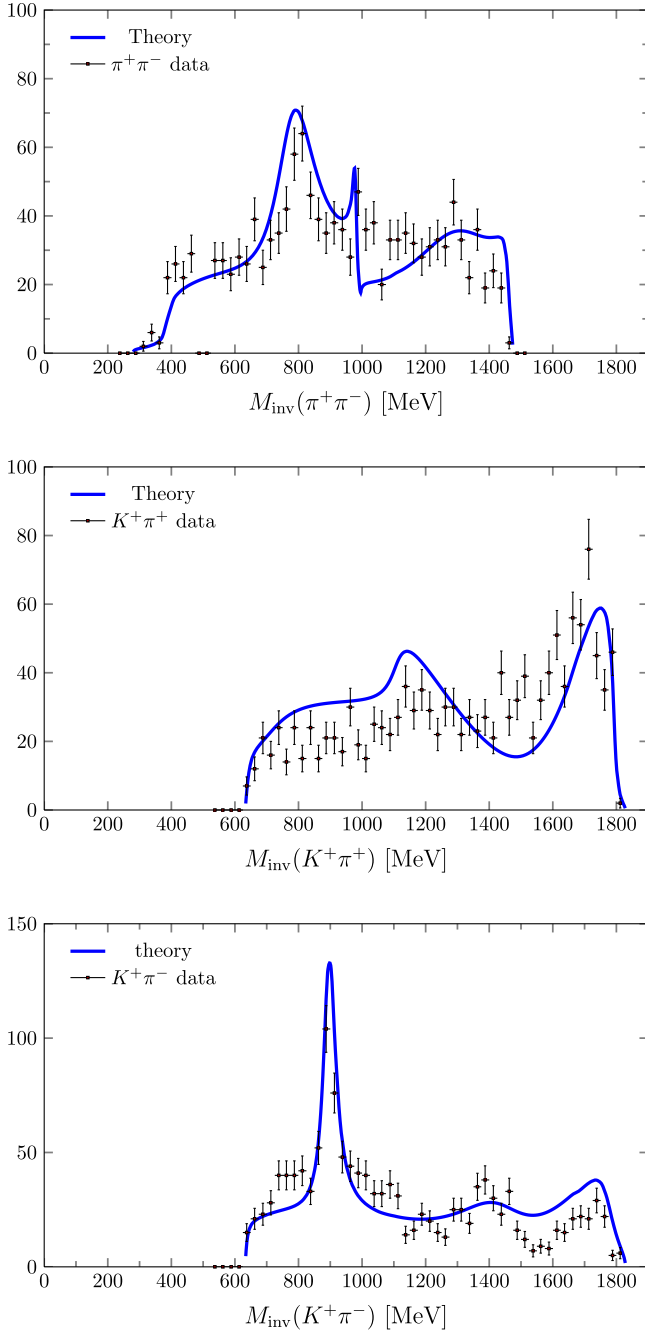
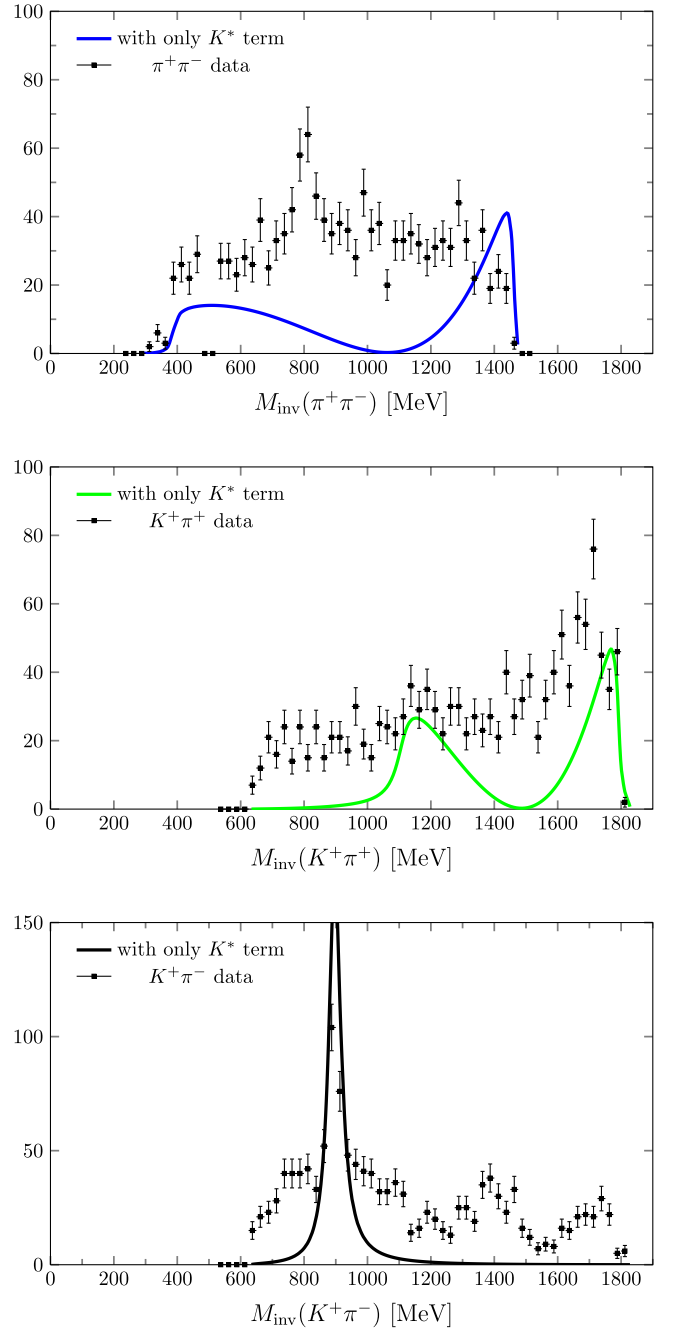


FIG. 12. Invariant mass distributions.

obtain is 3.68, indicating the discrepancies in some regions. The errors in the β and γ parameters are larger, indicating a minor role of the $K_0^*(1430)$ and $f_0(1370)$ resonances. Yet, we are not so much concerned about punctual discrepancies with the data, where other mechanisms could contribute, since our aim is to see the effect of the $f_0(500)$, $f_0(980)$, and $K_0^*(700)$ scalar resonances.

The $K_0^*(1430)$ contribution is observed as a soft peak in the $K^+\pi^-$ mass spectrum of Fig. 12 around 1400 MeV and the $f_0(1370)$, which has a very large width, shows up in the $\pi^+\pi^-$ spectrum in the region around 1200–1400 MeV,

FIG. 13. Invariant mass distributions obtained with the K^* term alone.

where otherwise there would be strength missing. On the other hand, the $f_0(500)$, $f_0(980)$, $K_0^*(700)$ have been introduced dynamically here, through the interaction of pseudoscalar pairs, and one can see their contribution in the low energy part of the $M_{\text{inv}}(\pi^+\pi^-)$ spectrum of Fig. 12 ($f_0(500)$), the sharp peak around 980 MeV ($f_0(980)$) in the same spectrum and the low energy part of the $K^+\pi^-$ mass spectrum ($K_0^*(700)$) in the same figure, respectively.

Technically, from the amplitude $t^{(2)}$, since the $K\bar{K}$, $\eta\eta$ come from the $s\bar{s}$ hadronization that has $I = 0$, we can

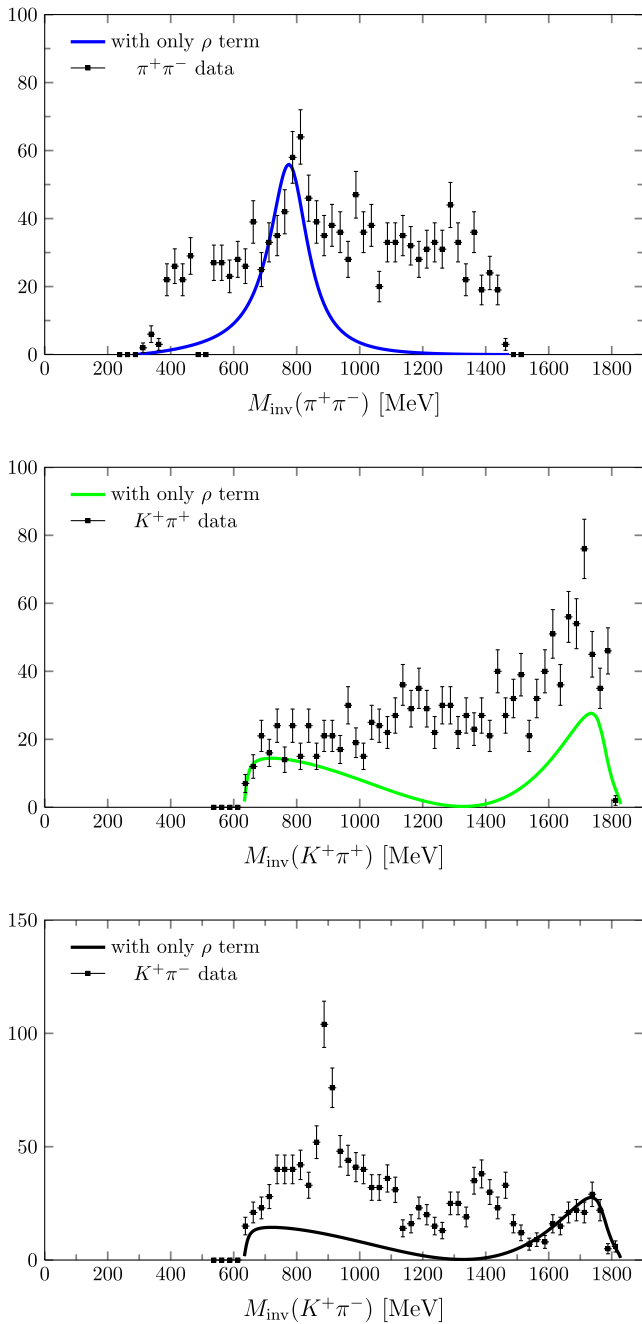


FIG. 14. Invariant mass distributions obtained with the ρ^0 term alone.

expect to obtain a contribution from the $f_0(980)$, which couples strongly to $K\bar{K}$ but weakly to $\pi\pi$, and to a minor extend a contribution from the $f_0(500)$ which couples to $\eta\eta$ but not strongly. On the other hand, from $t^{(4+6)}$ we get contribution both from $f_0(980)$ and $f_0(500)$ since now we have $\pi\pi$ intermediate states which couple strongly to $f_0(500)$. Furthermore, from $t^{(5)}$ we get a contribution from the scalar $K_0^*(700)$ resonance which couples to $K\pi$.

We should note that all these three resonance contributions have been included by means of a unique parameter,

h , up to a global normalization, and the fair reproduction of the spectra obtained in the relevant regions supports that these contributions are indeed correlated and our mechanism for production of these resonances produces a fair reproduction of their relative weight in these mass distributions.

In order to see the relevance of the scalar resonances in these spectra, it is interesting to see what distributions we obtain if we keep only the K^{*0} or the ρ^0 terms. This is shown in Figs. 13 and 14. We conduct two tests. In one case we keep only the K^* contribution. This means taking only the $t^{(1)}$ amplitude in Eq. (21). We observe in Fig. 13 that much of the strength in the $K^+\pi^-$ mass distribution outside the K^{*0} peak is not accounted for. On the other hand, it produces a two peak structure in the $K^+\pi^+$ distribution and also in the $\pi^+\pi^-$ one. These peaks are well known as reflections in some channels of resonances in another channel and should not be confused with signals of a new resonance. In Fig. 14 we repeat the exercise putting only the contribution of the ρ . This is done by taking only the $t^{(3)}$ amplitude in Eq. (21). Once again, we show that much strength outside the ρ region is not accounted for and, similarly to the case of the K^* resonance alone, the ρ peak generates reflections with two peaks, both in the $K^+\pi^+$ and $K^+\pi^-$ mass distributions.

IV. CONCLUSIONS

We have performed a fit to the three mass distributions of the $D_s^+ \rightarrow K^+\pi^+\pi^-$ reaction in which we have introduced empirically the contributions of the main decay channels, $D_s^+ \rightarrow K^+\rho^0$ and $D_s^+ \rightarrow K^{*0}\pi^0$. In addition, we also introduce empirically two other contributions from channels of smaller relevance, the $D_s^+ \rightarrow \pi^+K_0^*(1430)$ and $D_s^+ \rightarrow K^+f_0(1370)$. As to the $f_0(500)$, $f_0(980)$, and $K_0^*(700)$ resonances, they are not introduced as explicit amplitudes, but they are generated from the interaction of pseudoscalar mesons. For this purpose we look at the decay channels at the quark level and perform a hadronization of $q\bar{q}$ pairs to two mesons in order to produce three pseudoscalar mesons in the final state, and allow these mesons to interact by pairs to produce the desired final state. In this way the three light scalar mesons are introduced dynamically and their contributions are correlated by means of just one free parameter. We obtain a fair reproduction of the $\pi^+\pi^-$, $K^+\pi^-$ mass distributions in the regions where these resonances appear, and the relative weight of the contribution of the light scalar mesons also agrees with the measured spectra. While in other reactions [29–34] some of these resonances are produced in the same way, in each of them one sees one or two of the resonances discussed here. In the present case we see the three of them in the same reaction. Reproducing their effect by means of just one parameter adds extra support for the dynamically generated origin of these resonances, stemming from the interaction of pseudoscalar

mesons. Given the accumulated support from different reactions for the dynamical origin of the light scalar resonances, we can only encourage to use the present approach in future experimental analyses, which can reduce the number of parameters used, and help to get further insight on the dynamics of the reactions.

ACKNOWLEDGMENTS

We thank Bai-Cian Ke and Hai-Bo Li for providing us the experimental data. This work is partly supported by the National Natural Science Foundation of China under Grants No. 12175066, No. 11975009. This work is also supported by the Spanish Ministerio de Economía y

Competitividad (MINECO) and European FEDER funds under Contracts No. FIS2017-84038-C2-1-P B, No. PID2020-112777GB-I00, and by Generalitat Valenciana under contract PROMETEO/2020/023. This project has received funding from the European Union Horizon 2020 research and innovation programme under the Program No. H2020-INFRAIA-2018-1, Grant Agreement No. 824093 of the STRONG-2020 project. This research is also supported by the Munich Institute for Astro-, Particle and BioPhysics (MIAPbP) which is funded by the Deutsche Forschungsgemeinschaft (DFG, German Research Foundation) under Germany's Excellence Strategy-EXC-2094 -390783311.

-
- [1] H. Y. Cheng, *Phys. Rev. D* **67**, 034024 (2003).
 [2] I. Bediaga and M. Nielsen, *Phys. Rev. D* **68**, 036001 (2003).
 [3] D. R. Boito, J.-P. Dedonder, B. El-Bennich, O. Leitner, and B. Loiseau, *Phys. Rev. D* **79**, 034020 (2009).
 [4] B. El-Bennich, O. Leitner, J.-P. Dedonder, and B. Loiseau, *Phys. Rev. D* **79**, 076004 (2009).
 [5] F. S. Navarra, M. Nielsen, E. Oset, and T. Sekihara, *Phys. Rev. D* **92**, 014031 (2015).
 [6] T. Sekihara and E. Oset, *Phys. Rev. D* **92**, 054038 (2015).
 [7] J. M. Dias, F. S. Navarra, M. Nielsen, and E. Oset, *Phys. Rev. D* **94**, 096002 (2016).
 [8] W. Wang, *Phys. Lett. B* **759**, 501 (2016).
 [9] S. Sakai, E. Oset, and W. H. Liang, *Phys. Rev. D* **96**, 074025 (2017).
 [10] N. N. Achasov, A. V. Kiselev, and G. N. Shestakov, *Phys. Rev. D* **102**, 016022 (2020).
 [11] N. Ikeno, M. Bayar, and E. Oset, *Eur. Phys. J. C* **81**, 377 (2021).
 [12] Y. J. Shi and U. G. Meissner, *Eur. Phys. J. C* **81**, 412 (2021).
 [13] H. Y. Cheng, C. W. Chiang, and Z. Q. Zhang, *Phys. Rev. D* **105**, 033006 (2022).
 [14] E. Oset, W. H. Liang, M. Bayar, J. J. Xie, L. R. Dai, M. Albaladejo *et al.*, *Int. J. Mod. Phys. E* **25**, 1630001 (2016).
 [15] M. Diakonou and F. Diakonou, *Phys. Lett. B* **216**, 436 (1989).
 [16] J. A. Oller, *Phys. Rev. D* **71**, 054030 (2005).
 [17] D. R. Boito, P. C. Magalhães, M. R. Robilotta, and G. R. S. Zarnauskas, [arXiv:0805.4803](https://arxiv.org/abs/0805.4803).
 [18] D. R. Boito and R. Escribano, *Phys. Rev. D* **80**, 054007 (2009).
 [19] P. C. Magalhães, M. R. Robilotta, K. S. F. F. Guimarães, T. Frederico, W. de Paula, I. Bediaga, A. C. dos Reis, C. M. Maekawa, and G. R. S. Zarnauskas, *Phys. Rev. D* **84**, 094001 (2011).
 [20] K. S. F. F. Guimarães, O. Lourenço, W. de Paula, T. Frederico, and A. C. dos Reis, *J. High Energy Phys.* **08** (2014) 135.
 [21] J. P. Dedonder, R. Kaminski, L. Lesniak, and B. Loiseau, *Phys. Rev. D* **89**, 094018 (2014).
 [22] P. C. Magalhães and M. R. Robilotta, *Phys. Rev. D* **92**, 094005 (2015).
 [23] F. Niecknig and B. Kubis, *J. High Energy Phys.* **10** (2015) 142.
 [24] J. J. Xie, L. R. Dai, and E. Oset, *Phys. Lett. B* **742**, 363 (2015).
 [25] S. X. Nakamura, *Phys. Rev. D* **93**, 014005 (2016).
 [26] D. Boito, J. P. Dedonder, B. El-Bennich, R. Escribano, R. Kaminski, L. Lesniak, and B. Loiseau, *Phys. Rev. D* **96**, 113003 (2017).
 [27] F. Niecknig and B. Kubis, *Phys. Lett. B* **780**, 471 (2018).
 [28] E. Kou, T. Moskalets, and B. Moussallam, *J. High Energy Phys.* **12** (2023) 177.
 [29] G. Toledo, N. Ikeno, and E. Oset, *Eur. Phys. J. C* **81**, 268 (2021).
 [30] J. Y. Wang, M. Y. Duan, G. Y. Wang, D. M. Li, L. J. Liu, and E. Wang, *Phys. Lett. B* **821**, 136617 (2021).
 [31] X. Zhu, D. M. Li, E. Wang, L. S. Geng, and J. J. Xie, *Phys. Rev. D* **105**, 116010 (2022).
 [32] Z. Y. Wang, J. Y. Yi, Z. F. Sun, and C. W. Xiao, *Phys. Rev. D* **105**, 016025 (2022).
 [33] L. R. Dai, E. Oset, and L. S. Geng, *Eur. Phys. J. C* **82**, 225 (2022).
 [34] Xin Zhu, Hao-Nan Wang, De-Min Li, En Wang, Li-Sheng Geng, and Ju-Jun Xie, *Phys. Rev. D* **107**, 034001 (2023).
 [35] R. T. Aoude, P. C. Magalhães, A. C. Dos Reis, and M. R. Robilotta, *Phys. Rev. D* **98**, 056021 (2018).
 [36] J. P. Dedonder, R. Kamiński, L. Leśniak, and B. Loiseau, *Phys. Rev. D* **103**, 114028 (2021).
 [37] L. Roca and E. Oset, *Phys. Rev. D* **103**, 034020 (2021).
 [38] J. M. Link *et al.* (FOCUS Collaboration), *Phys. Lett. B* **601**, 10 (2004).
 [39] M. Ablikim *et al.* (BESIII Collaboration), *J. High Energy Phys.* **08** (2022) 196.
 [40] J. A. Oller, E. Oset, and A. Ramos, *Prog. Part. Nucl. Phys.* **45**, 157 (2000).
 [41] L.-L. Chau, *Phys. Rep.* **95**, 1 (1983).
 [42] A. Bramon, A. Grau, and G. Pancheri, *Phys. Lett. B* **345**, 263 (1995).

- [43] J. X. Lin, J. T. Li, S. J. Jiang, W. H. Liang, and E. Oset, *Eur. Phys. J. C* **81**, 1017 (2021).
- [44] M. Bando, T. Kugo, S. Uehara, K. Yamawaki, and T. Yanagida, *Phys. Rev. Lett.* **54**, 1215 (1985).
- [45] S. Furui, R. Kobayashi, and M. Nakagawa, *Nuovo Cimento Soc. Ital. Fis.* **108A**, 241 (1995).
- [46] U. G. Meissner, *Phys. Rep.* **161**, 213 (1988).
- [47] H. Nagahiro, L. Roca, A. Hosaka, and E. Oset, *Phys. Rev. D* **79**, 014015 (2009).
- [48] R. L. Workman *et al.* (Particle Data Group), *Prog. Theor. Exp. Phys.* **2022**, 083C01 (2022) and 2023 update.
- [49] R. Molina, D. Nicmorus, and E. Oset, *Phys. Rev. D* **78**, 114018 (2008).
- [50] L. S. Geng and E. Oset, *Phys. Rev. D* **79**, 074009 (2009).